A Multi-Task Deep Learning Approach for Sensor-based Human Activity Recognition and Segmentation

Furong Duan, Tao Zhu, *Member, IEEE*, Jinqiang Wang, Liming Chen, *Senior Member, IEEE,* Huansheng Ning, *Senior Member, IEEE,* and Yaping Wan

Abstract—Sensor-based human activity segmentation and recognition are two important and challenging problems in many real-world applications and they have drawn increasing attention from the deep learning community in recent years. Most of the existing deep learning works were designed based on pre-segmented sensor streams and they have treated activity segmentation and recognition as two separate tasks. In practice, performing data stream segmentation is very challenging. We believe that both activity segmentation and recognition may convey unique information which can complement each other to improve the performance of the two tasks. In this paper, we firstly proposes a new multitask deep neural network to solve the two tasks simultaneously. The proposed neural network adopts selective convolution and features multiscale windows to segment activities of long or short time durations. First, multiple windows of different scales are generated to center on each unit of the feature sequence. Then, the model is trained to predict, for each window, the activity class and the offset to the true activity boundaries. Finally, overlapping windows are filtered out by non-maximum suppression, and adjacent windows of the same activity are concatenated to complete the segmentation task. Extensive experiments were conducted on eight popular benchmarking datasets, and the results show that our proposed method outperforms the state-of-the-art methods both for activity recognition and segmentation.

Index Terms—Deep learning, Multitask learning, Activity recognition, Activity segmentation, Sensors

I. INTRODUCTION

S ENSOR-based activity segmentation and recognition algorithms have been widely employed in real-life applications, such as ambient-assisted living [1]–[3], human-computer interaction [4]–[6] and healthcare [7]–[9]. An activity segmentation algorithm concentrates on identifying the starting and ending positions of the activity, and an activity recognition algorithm aims to recognize the activities based on the data streams collected from the various sensors.

Furong Duan, Tao Zhu, Jinqiang Wang, and Yaping Wan were with the Department of Computer Science, University of South China, 421001 China (email: frduan@stu.usc.edu.cn, tzhu@usc.edu.cn, jqwang@stu.usc.edu.cn, yp-wan@aliyun.com).

Liming Chen was with the School of Computing and Mathematics, University of Ulster, Belfast, BT37 0QB, U.K. Huansheng Ning was Department of Computer & Communication Engineering, University of Science and Technology Beijing, 100083 China (email: l.chen@ulster.ac.uk, ninghuan-sheng@ustb.edu.cn).

In the field of activity segmentation, several approaches use a fixed window to segment the activity, and the selection of the segmented window length is based on experience. A large window contains more information about the data stream but may fail to identify activity transitions if there are different activities within the window. In contrast, a small window can quickly capture activity transitions but may lead to misclassifications because it does not contain enough information. To tackle this dilemma, some researchers try to adaptively determine the window length based on the probability of the signal belongs to a particular activity [10]. Some researchers proposed a time window based segmentation model and dynamically manipulated the model parameters to shrink or expand the time windowâĂŹs length [11].

In the field of activity recognition, many traditional machine learning algorithms, such as SVM, KNN and random forest, apply handcrafted statistical features to represent the characteristics of the data stream, and have achieved promising performances. However, extracting the effective features depends on domainnon expertise. Recently, deep learning techniques, which can automatically learn rich features, have been widely applied in sensor-based activity recognition tasks [12] [13]. CNNs [14], LSTM [15], DeepConvLSTM [16], and DeepConvLSTM-Attention [17] models have been demonstrated to improve the accuracy of activity recognition.

However, most of the earlier works are designed based on pre-segmented sensor streams and treat activity segmentation and recognition as two separate tasks. In real life, Since activities do not have a predefined sequence and duration, a pre-segmented offline segmentation technique is performed by examining all the datasets and therefore is not suitable for real-time applications.

Furthermore, if data segmentation is considered a preprocessing step, errors in data segmentation may propagate to the later steps [18]. We believe that both activity segmentation and recognition may convey unique information that can complement each other to improve the performance of activity segmentation and activity recognition. In this paper, we propose a novel multi-task framewok for simultaneously sensor based activity segmentation and recognition. The framewok is motivated by the SSD [19] method that exploited in the computer vision field. First, we generate multiple windows of different scales centered on each unit of the activity feature sequence. Second, we formulate a deep neural network to simultaneously predict the activity class contained in each

window and the offset of the window from the truth activity boundary. Next, considering the same surrounding activity, many predicted windows with high overlap may be output. we use the non-maximum suppression algorithm [20] to keep the appropriate window. Finally, we combine activity segmentation with activity recognition to jointly update the learnable parameters of the different components. The main contributions of this paper are summarized as follows:

- We propose a novel multi-task framewok, denoted by MTHARS, which can effectively combine activity segmentation and recognition to improve the performance of two tasks.
- Taking the dynamics of activity length, we propose a multiple scale windows concatenation method to segment activities of various length.
- We use eight popular benchmarking activity datasets for the activity segmentation and recognition experiments. The experimental results show that MTHARS performs better than the state-of-the-art methods. An ablation study is to analyze the effects of several key factors.

The rest of the paper is organized as follows. Section II describes related works. Section III the proposed method. Section IV presents the eight popular benchmarking datasets and the experimental setup, specifically, the experimental results for the activity segmentation and recognition and the ablation study. Section V summarizes our work and discusses future work.

II. RELATED WORK

In this section, related works are presented from two aspects, activity segmentation and activity recognition.

A. Activity Segmentation

Change point detection(CPD) based methods are used to detect the point in time when the behavior of a time series abruptly changes [21]. When a supervised approach is employed for change point detection, machine learning algorithms can be trained as binary or multi-class classifiers [22]. [23] proposed computing several most likely fragment candidates based on the reversibility of the time series data.

The sliding window-based sensor data stream segmentation method is a common method for segmenting sensor data streams. A fixed window length is used to proportion the data stream into the same size segments for input into the model for activity recognition. The window length determines the length of each data segment, which directly affects the quality of the feature extractions and the accuracy of the classifications performed by the model [24]. Many strategies for segmenting sensor data based on sliding windows have been proposed.

Wang et al. [25] divided the entire sequence of sensor events into equal size time intervals. Banos et al. [26] experimented with various window sizes ranging from 0.25 s to 7 s in steps of 0.25 s on different activities. However, since the various activities are completed in different time periods, defining the optimal window size is challenging.

Aminikhanghahi and Cook [21] proposed that the sliding window length should be determined by whether there is a sufficient difference between the adjacent windows. Okeyo and Liming Chen [11] presented a time window based segmentation model and dynamically manipulated the model parameters to shrink or expand the time windowâĂŹs length. WanJie et al. [27] adopted a dynamic segmentation approach that identifies simple actions using both the sensor and time correlations. Noor and Mohd Halim Mohd [10] recommended that the window be automatically resized based on the activity signal distribution. Hong Li et al. [28] recommended starting with a fixed sliding window and then adjusting the window length based on various activities. Santos et al. [29] proposed a dynamically adaptive sliding window method, whose window length and overlap are continuously adjusted based on entropy feedback. Congcong et al. [30] proposed to detect the signal difference between time windows using multivariate gaussian distribution.

JuanYe et al. [31] proposed a new knowledge-driven concurrent activity recognition(KCAR) approach. In KCAR, the basic semantics of sensor events and the semantic similarity are investigated by dividing a continuous sensor sequence into different segments, each corresponding to an ongoing activity. Triboan and Liming Chen [32] applied a semantic-based approach which use ontologies to perform terminology box and assertion box reasoning, along with logical rules to infer whether the incoming sensor event is associated with a given sequences of the activity. Triboan and Liming Chen [33] proposed a semantics-based method to perform sensor data segmentation by combining generic knowledge and resident-specific preferences to facilitate the segmentation process.

B. Activity Recognition

In the field of activity recognition, CNNs consist of a convolutional, pooling layer and a fully connected layer that can learn unique representations. Ronao and Cho [14] proposed a convnet composed of alter-nating convolution and pooling layers. The basic features were extracted at the lower levels, and the more complicated features were extracted at the higher levels. Bianchi et al. [34] adopted a CNN model that consists of four convolutional layers and a fully connected layer for recognizing activities. Manuel et al. [35] proposed a new CNNs structure considering sensor-independent handling. Pham et al. [36] designed a senscapsnet approach that is suitable for spatial-temporal data. Cruciani et al. [37] proposed using a CNN to recognize activity based on sensors and audio for better extraction of the temporal features in activity data. Huang et al. [38] presented a shallower CNN implementation of the information interaction between channels in HAR scenarios, in which graph convolution is employed to implement the information interaction between the channels.

To better learn the temporal and spatial aspects of the activity data, OrdÃşÃśez et al. [16] suggests the use of a CNN mixed with LSTM layers. Cheng et al. [39] proposed a InnoHAR model which combine inception neural network and RNN. Xia et al. [40] presented that two layers of an LSTM were utilized to extract the temporal data features, followed by two levels of convolution and a combination of pooling layers and a BatchNorm between the convolution layers to extract the
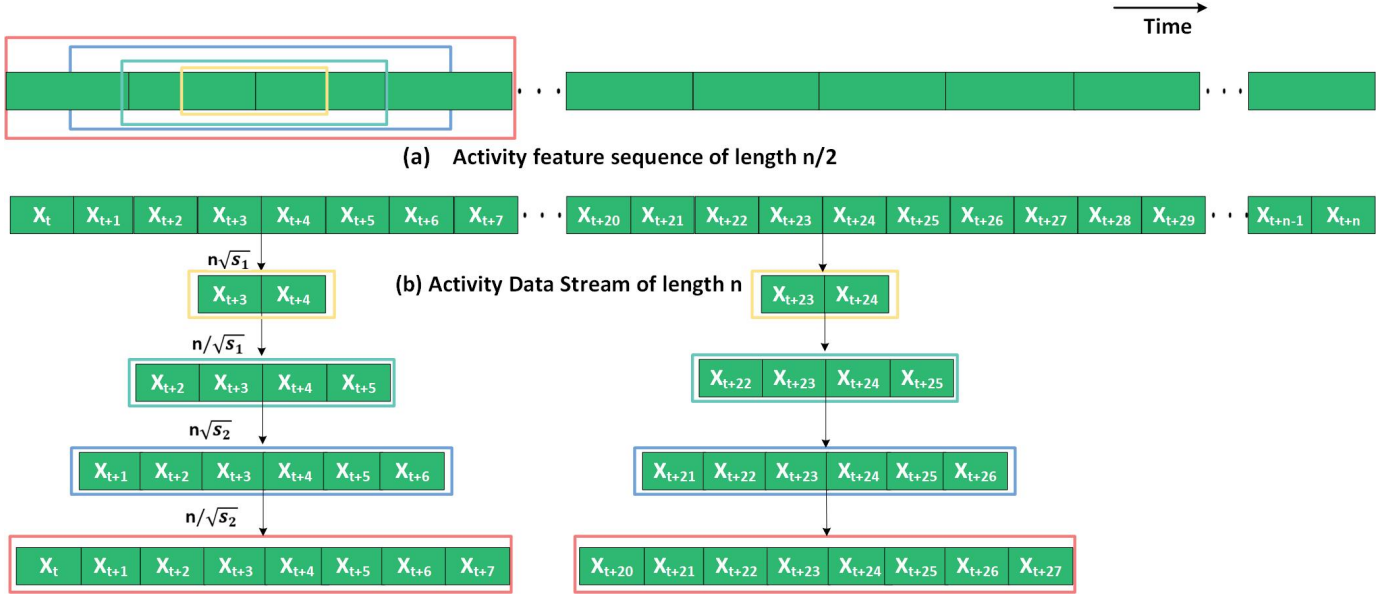
Fig. 1. (a) We generate four windows of different scales on the feature sequence, with each unit as the center of the window. (b) Four windows of different scales are generated centered on each data point. (The four colors represent the four different lengths of windows.)

spatial features. Tong et al. [41] proposed using the Bi-GRU-Inception model to learn the temporal features using a GRU network and Inception to analyze the spatial features between multiple channels.

In recent years, attention mechanisms have been investigated for deep HAR models. Y. Tang et al. [42] offers a ternary attention mechanism that includes three separate attention branches for the channel, time and sensor modalities. Zanobya et al. [43] posits that generating multiple heads with attention is more advantageous for improving convolutional feature representations, and each head in the multihead model is made up of two convolutional blocks. Existing models that use CNNs for activity recognition typically have the same receptive field size in the neurons of the same layer, limiting the possibility of capturing more features of different sizes in the same stage [44]. Using the varying size of the receptive fields on top of the feature maps at different scales was proposed early in computer vision to capture more valuable information. As a result, [44] presented SK convolution, which uses the attention approach to learn multiscale features by modifying the size of the perceptual field automatically to learn features of different scales.

III. MTHARS METHODOLOGY

In this section, we provide details of the problem definition and proposed MTHARS method inspired by SSD [19] that exploited in the computer vision field. There are four main components: multiscale window generation and matching, non-maximum suppression, model architecture, and model training.

A. Problem definition

Given a stream of activity data $\mathbf{X} = \{\mathbf{x_i}\}_{i=1}^{N}$, where $\mathbf{x_i}$ denotes a vector of signals collected at timestamp t. $\mathbf{a} =$ $\{a_k\}_{k=1}^{K}$ represents the K activity labels in the stream of activity data, where $a_k \in \{, A_2, A_3 \cdots A_L\}$. The duration of each a_k is different. Our goal is to segment the activity data into K nonoverlapping segments $\{\mathbf{X}_k\}_{k=1}^{K}$, each $\mathbf{X}_k \subseteq \mathbf{X}$, and $\bigcup_{k=1}^{k=K} \mathbf{X}_k = \mathbf{X}$. each $\mathbf{X}_k$ is assigned an activity a_k. The start and end of $\mathbf{X}_k$ represent the activity boundary of the corresponding activity. The activity boundary can be converted to the form of a center coordinate and length (t^x, t^l)

B. Multiscale windows

Representation of the window: Unlike the conventional sliding window used in activity recognition, we leverage computer vision's anchor concept. A window is denoted by (x, l), where x is the data point denoting the center position of a window, and l represents the length of the window.

Generation of windows: Assume that the provided activity data length is n. With a scale of $s \in (0, 1]$, We generate windows of various lengths centered on each data point of the activity data. $n\sqrt{s}$ and $n/\sqrt{s}$ are the generated window lengths. We can use a variety of scales to build several windows of various lengths. s takes the values of $s_1, s_2 \cdots s_m$. When using these scales to generate windows of different lengths centered at each data point, this will generate $n \times m \times 2$ windows. In this way, we generate multiple windows of different lengths to cover all the truth activity with various lengths as much as possible. As seen in Fig. 1, we generated four windows of different lengths centered on each data point.

As mentioned above, we generate multiple windows centered on each data point of the input data stream. However, by directly generating windows at the center of each data point, we will end up with many windows to calculate. Consider a data stream of length 600 if we generate 4 windows of different lengths centered on each data point. We need to predict 2400 windows on the data stream. To simplify the computational complexity, we use the receptive field in
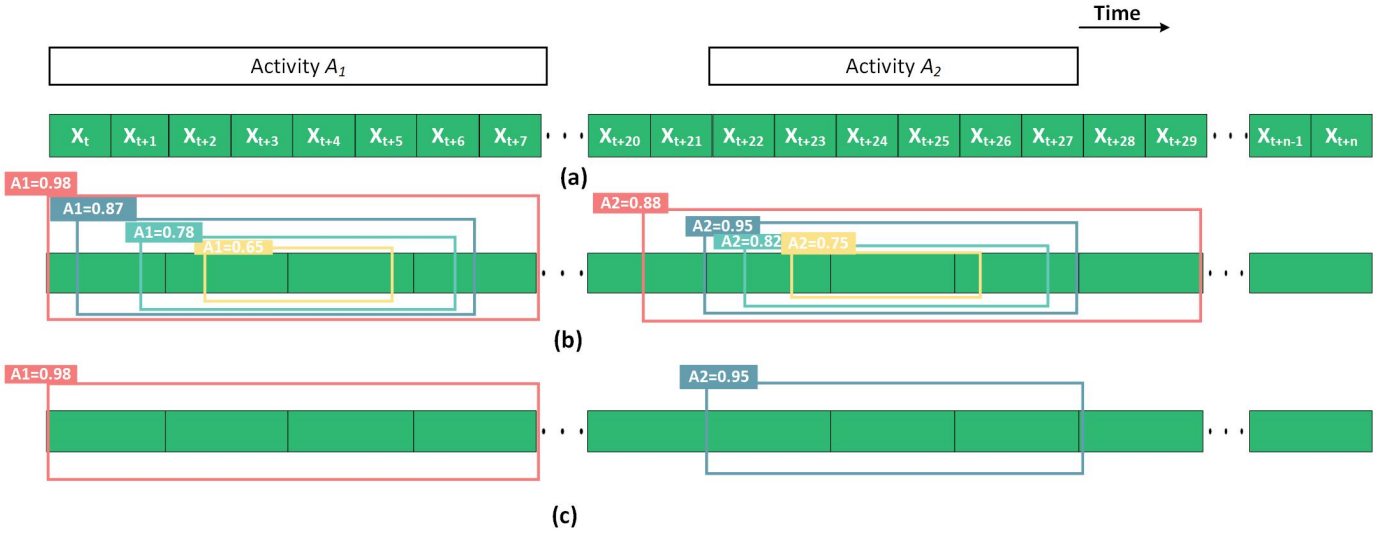
Fig. 2. (a) Activity data streams with truth activity boundaries. (b) Windows of different lengths with class probabilities. For example, $A_1 = 0.98$ represents a class probability of 0.98 for activity A_1 in this window. (c) Final maintained activity windows by the non-maximum suppression algorithm.

convolutional operations for guidance. Following its insight, by defining the length of the feature sequence generated from the backone network, we are able to determine the center of a uniformly sampled window on any data stream. Therefore, we generate windows centered on each unit of the feature sequence(As seen in Fig. 1) and divide the center of the window by the length of the feature sequence. Therefore, the value of x indicates the relative position of the window in the feature sequence. Since the centers of the window are distributed over all the units of the feature sequence, these centers are uniformly distributed over any input data stream based on their relative spatial locations.

IOU: We employ the Jaccard index to measure the similarity between the generated window and the truth activity bounding. The Jaccard index is defined as the ratio of the intersection length of the window and the true activity bounding box to their merge length. For windows and truth activity boundaries, we denote their Jaccard values as an intersection over union (IOU). The range of an IOU is a number between 0 and 1 that indicates whether there is any overlap. A value of 0 indicates that there is no overlap, while a value of 1 indicates that they are equal. For example, given windows $W_1(5, 10)$, $W_2(30, 50)$, and truth activity bounding box $T_1(40, 60)$, the IOU of W_1 and T_1 is 0, and the IOU of W_2 and T_1 is 0.69.

Multiscale window labeling and matching: During the training process, each generated window is treated as a training sample. To train the model, we must label each window with an activity class and a bounding offset, where the former refers to the activity associated with the window and the latter refers to the offset of the truth activity bounding box in relation to the window. We generate multiple windows of various lengths for the feature sequence. Next, we predict the activity class and boundary offset of all the windows, then we adjust their length according to the predicted offsets to better obtain the predicted window. Finally, we only output the predicted activity windows that satisfy the criteria. We

labeled the training set with the true activity boundary location and the class. To mark any generated window, we refer to the labeled position and class of its assigned truth activity bounding box closest to the window. We apply the following method to assign the closest truth activity bounding box to the window.

Assume the generated windows are $W_1, W_2 \cdots, W_{na}$, and the truth activity bounding boxes are $T_1, T_2 \cdots, T_{nb}$, where $na > nb$. First, we create a matrix $\mathbf{M} \in \mathbb{R}^{(n_a \times n_b)}$, in which the element m_{ij} in the ith row and j^{th} column is the IOU of the window W_i and the truth activity bounding boxes T_j. The method's steps are as follows:

- Finding the largest element in matrix $\mathbf{M}$, we set its row index and column index to i_1 and j_1, respectively, and then assign the truth activity bounding box T_{j_1} to the generated window W_{i_1}, discarding all the elements in the i_1 rows and j_1 columns of the matrix $\mathbf{M}$ after the first assignment.
- Find the largest value of the remaining elements in matrix M. i_2, j_2 are the row and column indices, respectively. We assign the generated window W_{i_2} to the truth activity bounding box T_{j_2} and discard the i_2 row and all the elements in the j_2 column.
- Next, we repeat the previous steps until all of the entries in column nb of the matrix $\mathbf{M}$ have been discarded. At that time, all of the true activity bounding boxes have been allocated a generated window.
- Finally, we iterate the remaining na-nb windows one by one. If we identify the true activity bounding box T_j with the largest ratio to the window IOU in row i of the matrix $\mathbf{M}$ and the ratio is greater than the threshold value, we assign the true activity bounding box T_j to window W_i.

For better comprehension of the process, we provide a concrete example to illustrate the process of assigning the generated window to the truth activity bounding box. Considering that the greatest IOU ratio in the matrix $\mathbf{M} \in \mathbb{R}^{(5 \times 3)}$ is m_{51}, the

truth activity bounding box T_1 is assigned to the window W_5. Then, we discard all the elements in Row 5 and Column 1 of the matrix **M**.

$$\mathbf{M} = \begin{bmatrix} 0.55 & 0.82 & \mathbf{0.96} \\ 0.69 & \mathbf{0.95} & 0.78 \\ 0.32 & 0.48 & 0.88 \\ 0.75 & 0.67 & 0.45 \\ \mathbf{0.98} & 0.67 & 0.88 \end{bmatrix}_{5 \times 3}$$

Then, we find the maximum m_{13} in the remaining region of the matrix, assign the truth activity bounding box T_3 to the window W_1, and discard all the elements in Row 1 and Column 3 of the matrix. Next, we choose the largest m_{22} in the remaining part of the matrix to allocate the truth activity bounding box T_2 to the window W_2 and discard all the components in Row 2 and Column 2. After that, we just need to iterate through the remaining unassigned windows W_3, W_4 and assign them a truth activity bounding box based on whether their IOU values with the truth bounding box are greater than the threshold.

5. We assign the truth activity bounding box to the generated windows. Then, we proceed to annotate the activity class and offset with the following approach. If a window is assigned to a truth activity bounding box, the class of the window will be labeled as that of a truth activity bounding box. The following method is used to compute the true offset.

Given a truth activity bounding box $T = (t^x, t^l)$ and a window $W = (w^x, w^l)$. We define the offset as (f^x, f^l), where f^x, f^l represents the center offset and the length offset, respectively, calculated as follows:

$$f^x = \frac{t^x - w^x}{w^l} \tag{1}$$

$$f^l = \log \frac{t^l}{w^l} \tag{2}$$

Predicted activity boundary: In the predicting process, we generate multiple windows for each activity and predict the activity class and offsets for each window. The offsets (f^x, f^l) are obtained by the Recognition and Segmentation NetWork (as in Fig 3). We employ the predicted offsets to calculate the predicted activity boundary $(\hat{t}^x, \hat{t}^l)$ in the following way, where $\hat{t}^x, \hat{t}^l$ denote the activity center and length, respectively.

$$\hat{t}^x = f^x w^l + w^x \tag{3}$$

$$\hat{t}^l = w^l \exp(f^l) \tag{4}$$

For example, provided the activity data stream $\mathbf{X} = \{\mathbf{x_i}\}_{i=1}^{N}$, we predict that the boundaries of activities A_1 and A_2 are (100, 200) and (152, 304), respectively, and we can also represent the activity boundary by transforming A and B into the form of the starting position and the ending position, such as (1, 201) and (202, 506). Therefore, $\{\mathbf{x_i}\}_{i=1}^{201}$ $\{\mathbf{x_i}\}_{i=202}^{506}$ are the activities A_1 and A_2, respectively.

Non-maximum Suppression (NMS): When there are so many windows present, for the same surrounding activity, many predicted windows with high overlap may be output. To simplify the output, we can merge similar windows belonging to the same activity by using a non-maximum suppression algorithm.

The following is the non-maximum suppression algorithm procedure. For a predicted window W, the Recognition and Segmentation NetWork predicts a probability c for each activity class. The maximum probability c is used to denote the activity class probability corresponding to the window W (as shown in Fig.2). Within the same activity, all the predicted windows are sorted by class probability c in descending order and organized in the form of a list L. Then, we process this sorted list L as follows.

- Select the window W_1 with the highest class probability c as the base window and remove the rest of the windows with W_1 IOU values exceeding the threshold. Thus, the window W_1 with the highest c is retained, and the windows with high similarity to W_1 are discarded. In other words, the window with the non-highest class probability is suppressed.
- The window W_2 with the second highest class probability c is selected as another base window, and the remaining window with W_2, where the IOU value exceeds the threshold is deleted.
- Repeat the above steps until all windows are selected as base windows or discarded. In this way, the IOU values of any two predicted windows are below the threshold.

C. Model

The MTHARS approach consists of the SK network [44] (as a backone network), the Windows Generate module and the recognition and segmentation module, as shown in Fig. 3. The parameters are presented in Table I. First, the feature sequence is generated via the backone network. Then, the Windows Generate module generates a certain number of windows according to the length of the feature sequence. The recognition and segmentation module predicts the activity class contained in each window and the offset between the window and the truth activity bounding box. Then, a non-maximum suppression algorithm is used to retain the final satisfactory windows.

D. Recognition and Segmentation Module

The module is a network comprised of two branches for offset and class prediction. For the class prediction branch, suppose the number of activity classes is k, and each generated window has $k+1$ classes, where class 0 represents the background. The length of the feature sequence is n. When centered on each unit of the feature sequence generating m windows, a set of $n \times m \times 2$ windows need to be classified. If we choose a fully connected layer, it is easy to generate too many model parameters; therefore, we choose a convolutional layer. Specifically, the class prediction branch uses a convolutional layer that does not change the length of the feature sequence. By this means, the output and input coordinates correspond to each other in the length of the feature sequence. Consider the input and output for the same x coordinate: The class predictions of all the windows centered on the x-coordinate of the input feature sequence are stored in the channel at the x-coordinate of the output feature sequence. For class prediction,
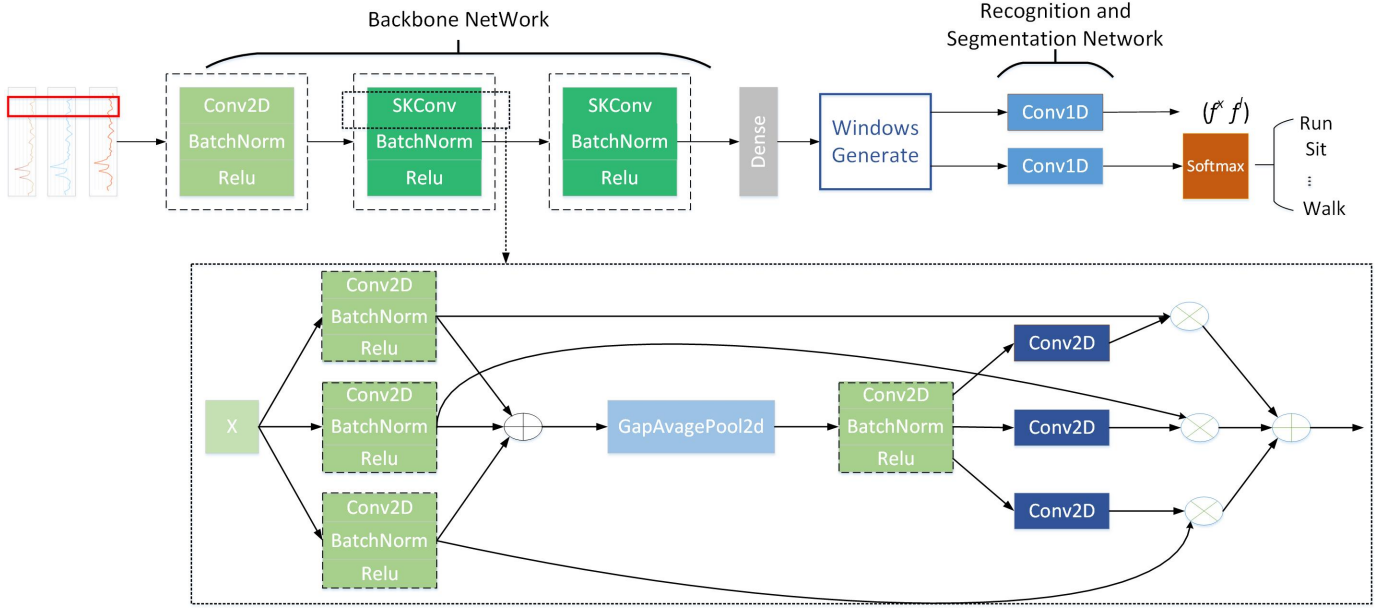
Fig. 3. Overview of the Proposed MTHARS Network Architecture

TABLE I
SIMPLE PARAMETER DESCRIPTION OF THE MTHARS

Layers	Parameters		
Layer1	Conv2D(5×1 / 3×1 / 1×0)		
SKConv	Conv2D(3×1 / 1×1 / 1×1 / 1×1)	Conv2D(3×1 / 1×1 / 2×1 / 2×1)	Conv2D(3×1 / 1×1 / 3×1 / 3×1)
	Conv2D (1 × 1 / 1×1)		
	Conv2D (1 × 1 / 1×1)	Conv2D (1 × 1 / 1×1)	Conv2D (1 × 1 / 1×1)
Recognition and Segmentation	Conv1D (3 × 3 / 1×1 / 1×1)	Conv1D (3 × 3 / 1×1 / 1×1)	

[1] (3×1 / 1×1 / 1×1 / 1×1) represents kernel size, stride, padding, and dilation in order.

there are $m(k+1)$ output class channels, with the index of the channel $i(k+1)+j$ $(0 \leq j \leq k)$ representing the class index j predictions for the window index i. The design of the offset prediction is similar to that of the class prediction. The only difference is that we predict two offsets for each window instead of $k+1$ activity classes.

E. Training Model

During the forward propagation of the model, we generate multiscale windows and predict their activity classes and window offsets. The truth activity class and truth offset are labeled on each generated window using the label information. Finally, we calculate the loss based on the predicted classes and offsets with the true classes and offset values, respectively. The offset loss (5) is calculated by comparing the ground truth offset $f = (f^x, f^l)$ with the predicted offset $\hat{f} = (f^x, f^l)$ using $Smooth_{L_1}$ loss.

$$L_{loc}(f, \hat{f}) = \sum_{i \in \{x,l\}} Smooth_{L1}(f^i - \hat{f}^i) \quad (5)$$

in which

$$Smooth_{L1}(x) = \begin{cases} 0.5(x)^2, if|x| < 1. \\ |x| - 0.5, otherwise. \end{cases} \quad (6)$$

The class loss is calculated by the window labeled activity class **a** with the predicted class **â** using cross-entropy loss (7), in which n represents the sample number.

$$L_{conf}(\mathbf{a}, \hat{\mathbf{a}}) = -\sum_{i=1}^{n} a_i log(\hat{a}_i) \quad (7)$$

Due to the limited number of activities, there will be many windows that are not matched with any of the activities after matching the window with the truth activity boundary, and these windows are referred to as negative samples. We sort all the negative samples in descending order according to the activity class probability and select a certain number of negative samples with a higher class probabilities to participate in the class loss calculation, with the number of negative samples to the number of positive samples in the ratio of 3:1. If all the negative samples are involved in the training, it will

Algorithm 1 Concatenate algorithm

Input: Predicted Activity boundary offset $\mathbf{F} = \{\mathbf{f}_i^x, \mathbf{f}_i^l\}_{i=1}^N$
　　Window $\mathbf{W} = \{\mathbf{w}_i^x, \mathbf{w}_i^l\}_{i=1}^N$
　　Predicted activity probability of the activity boundary $\mathbf{c} = \{c_i\}_{i=1}^N$,
　　Predicted activity class of the activity boundary $\mathbf{y} = \{y_i\}_{i=1}^N$,
Output: A set of activity boundaries $\mathcal{T} = \{(s_i, e_i)\}_{i=1}^K$ associated with activity class $\mathbf{a} = \{a_i\}_{i=1}^K$.
1: Remove redundant windows via the NMS algorithm
2: Calculate Eq. (3)(4) to obtain Predicted activity boundaries $\mathbf{P} = \{P_i\}_{i=1}^L$
3: $a_1 \leftarrow$ The first activity class in the first segment
4: $s_1 \leftarrow$ The starting position of the first activity in the first segment
5: $e_1 \leftarrow$ The ending position of the first activity in the first segment
6: Initial index i
7: **for** $j = 1$ to L **do**
8: 　**if** $a_1 \neq a_j$ **then**
9: 　　Add a_1 to a_i
10: 　　Add (s_1, e_1) to $\mathcal{T}_i$
11: 　　$a_1 \leftarrow a_j$
12: 　　$s_1 \leftarrow e_1 + 1$
13: 　　$i \leftarrow i + 1$
14: 　**end if**
15: 　$e_1 \leftarrow$ boundary length of $P_j + s_1$
16: **end for**
17: **if** $\mathcal{T}$ is Empty **then**
18: 　Add a_1 to a_i
19: 　Add (s_1, e_1) to $\mathcal{T}_i$
20: **end if**

---

make the network training process tend towards the negative samples.

Finally, we multiply the weight α by the class loss (conf) plus the weight β by the localization loss (loc).

$$L(a, \hat{a}, f, \hat{f}) = \frac{1}{N}(\alpha L_{conf}(a, \hat{a}) + \beta L_{loc}(f, \hat{f})). \quad (8)$$

F. Prediction

Since the length of the activity input to the network is fixed, we input a fixed length activity data stream at a time to recognize the start and end positions of each activity in each segment. Finally, we concatenate all the segments according to the activity class to obtain the start and end positions of each activity in the whole activity data stream. The concatenation algorithm is described in algorithm 1.

IV. EXPERIMENTS AND RESULTS

In this section, we detail our experiments and analyze the experimental results. We conduct an extensive experiment on eight benchmarking datasets to evaluate the effectiveness and scalability of our proposed MTHARS.

A. Datasets

We use eight publicly benchmark HAR datasets to assess the effectiveness of our system in daily activity segmentation and recognition. To make a fair comparison with other researchers, we select the same parameter values adopted by them. The specifics of the eight benchmark data we use are described in Table II, and the length interval distribution of benchmarking datasets is depicted in Fig. 4.

- SKODA Dataset [45]: A participant wearing 10 USB acceleration sensors in the upper and lower left and right hands, respectively, performed 10 different gestural activities in an automobile repair scenario for 3 hours. Each of the ten gesture actions, such as checking the gasoline tank, was completed more than 70 times.
- HCI Dataset [46]: Eight accelerometer USB sensors were worn on the lower and upper half of one participant's right arm to perform various gestural activities, such as sketching triangles, squares, and circles. More than 10 freehand movements and over 60 guided gestures were performed.
- PS Dataset [47]: Four participants recorded their walking, standing, standing, going upstairs, and going downstairs activities. They employed the phone's built-in accelerometer, magnetometer, and gyroscope by placing a mobile phone in four different locations on the body: pants pocket, waistband, right arm, and right wrist.
- WISDM Dataset [48]: The data were obtained by 29 participants using phones with triaxial acceleration sensors placed in their pant pockets with a sampling frequency of 20 Hz. Walking, strolling, walking up stairs, walking down stairs, standing motionless and standing up were among the six daily activities undertaken by each participant. The mean value of the column was used to fill in the missing values in the dataset.
- UCI Dataset [49]: The dataset consisted of 30 participants aged 19 to 48 years performing a series of daily activities. Each participant wore a Samsung Galaxy S2 smartphone around their waist and collected sensor data in 9 dimensions using the phone's built-in acceleration, gyroscope, linear acceleration and 3-axis angular velocity sensors and performed 6 different activities of daily living (walking, walking up stairs, walking down stairs, standing still, standing, and lying down).
- OPPORTUNITY Dataset [49]: IMU sensors were placed on 12 different places of each volunteer's body, and they were asked to repeat a sequence of 17 morning activities in the kitchen, such as opening the refrigerator door, closing the refrigerator door, opening the drawer, closing the drawer, and so on. Interpolation was performed to fill in missing values in the dataset.
- PAMAP2 Dataset [50]: Each of the nine participants wore an IMU on their chest, hands, and ankles, which collected acceleration, angular velocity, and magnetic force sensor information. Each participant was required to complete 12 mandatory activities, such as lying, standing, and walking up and down stairs, as well as six elective activities, such as watching television, driving, and playing ball. Due to

TABLE II
SIMPLE DESCRIPTION OF PUBLIC HAR DATASETS.

Attribute \ Dataset	SKODA	HCI	PS	WISDM	UCI	OPPORTUNITY	PAMAP2	UNIMIB SHAR
Type	AG	AG	ADL	ADL	ADL	ADL	ADL	ADL
Subject	1	1	4	29	30	4	9	4
Rate	96HZ	96HZ	50HZ	20HZ	50HZ	30HZ	33.3HZ	30HZ
WindowSize	1s	1s	2s	10s	2.56s	1s	1s	1s
Activity Categories	10	8	6	6	6	18	18	17
Sample	696975	7352	161959	1,098,208	748406	701366	2872533	11771

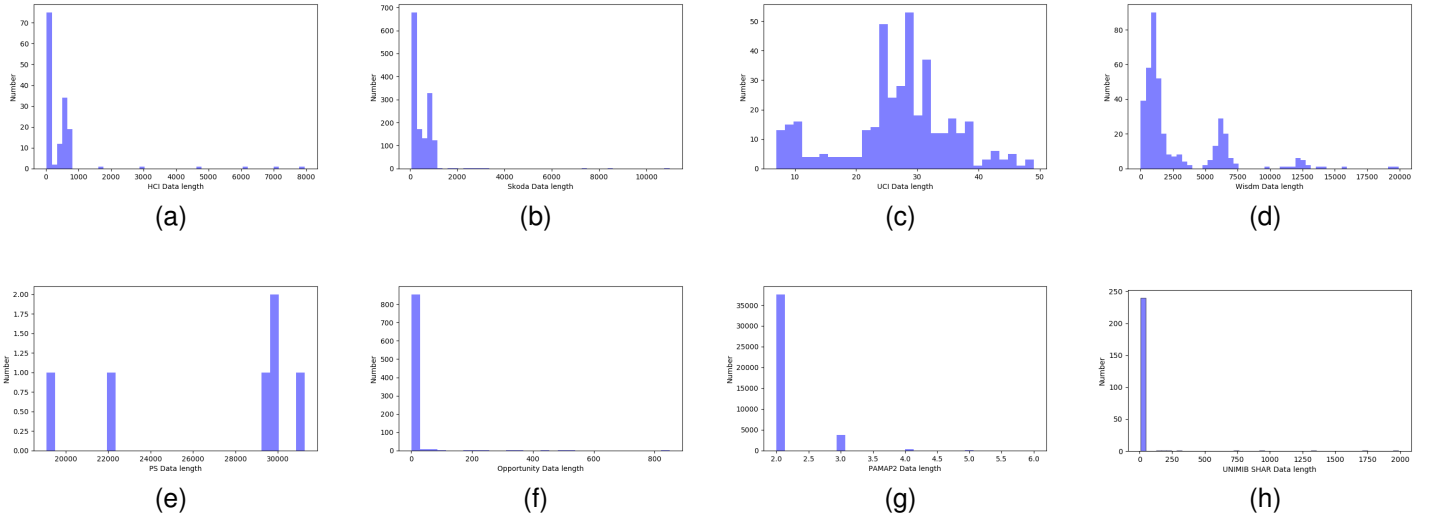[1] AG denotes gesture activity and ADL denotes activity of daily life.

Fig. 4. Activity length distribution of benchmarking datasets

interference generated during the activity transformation, the start and the last 10 s of each activity were eliminated to reduce the noise in the data for each type of activity.

- UNIMIB SHAR Dataset [51]: The dataset was collected by researchers from the University of Milano-Bicocca. The researchers equipped each of the 30 volunteers with Bosh BMA220 sensor Samsung cell phones and placed them in the participants' left or right pockets to collect activities of daily life (running, going upstairs, standing, walking, etc.) as well as different falling activities. Each activity was repeated 3 to 6 times.

B. Evaluation metric

To assess the accuracy of the activity segmentation, we use the Normalized Edit Distance (NED) [52]. NED uses the Levenshtein distance to measure how far apart the predicted activity sequence ($\hat{T}$) is from the truth activity sequence (T), calculated by the smallest operation that makes the two sequences equivalent, and NED is defined as follows.

$$NED = \frac{lev(\hat{T}, T)}{length\,of\,T} \quad (9)$$

$$lev(i,j) = \begin{cases} \max(i,j) \min(i,j) = 0 \\ min = \begin{cases} lev(i-1,j)+1 \\ lev(i,j-1)+1 \\ lev(i-1,j-1)+1_{i \neq j}. \end{cases} \end{cases} \quad (10)$$

Equation (10) is the smallest number of operation steps required to make the predicted sequence and the truth sequence equal, that takes into account three different ways to make the two sequences equal, namely, removing an element from the sequence, inserting a new one, and changing the sequence's label directly. This metric allows us to calculate the difference between the predicted activity boundary and the true activity boundary.

For an evaluation of activity recognition accuracy, since the activity classes in human activity data are mostly unbalanced, using classification accuracy is not an appropriate criterion to evaluate the classification performance [16]. Therefore, we apply F_1 to evaluate the effectiveness of activity classification.

$$F_1 = 2 \sum \frac{N_c}{N_{total}} \frac{P \times R}{P + R} \quad (11)$$

N_c represents the number of class c in all the samples, and N_{total} denotes the number of all the samples. *P* and *R* are calculated from the set of all positive classes, defined as below.

$$P = \frac{\sum_{i=1}^{n} TP_i}{\sum_{i=1}^{n} TP_i + \sum_{i=1}^{n} FP_i} \quad (12)$$

$$R = \frac{\sum_{i=1}^{n} TP_i}{\sum_{i=1}^{n} TP_i + \sum_{i=1}^{n} FN_i} \quad (13)$$

The activity class in the dataset is represented by *i*. TP_i represents the true positive class, FP_i denotes the false-positive class, and FN_i indicates the false-positive class.

C. Static Sliding-Window Segmentation

In this section, to investigate the effect of the static window segmentation methods, we use time-based sliding windows for experiments. As mentioned above, a time-based sliding window referrs to segmenting the activity data stream into the same length of time. The segmented data are randomly split into training and testing with a ratio of 70%, 30%. We used the commonly used time duration *t* from 1 to 10 s.

TABLE III
F_1 SCORE OF STATIC TIME-BASED SLIDING WINDOW.

Datasets	Methods	*t* = 1s	*t* = 2s	*t* = 3s	*t* = 5s	*t* = 10s
	NB	0.6351	0.6691	0.6027	**0.8292**	0.8123
	DT	0.8540	0.8928	0.9202	0.9364	**0.9657**
SKODA	SVM	0.8496	0.8830	**0.9461**	0.9065	0.9340
	LSTM	0.8656	0.8756	0.9122	**0.9336**	**0.9336**
	GRU	**0.8605**	0.8367	0.7932	0.7563	0.8435
	NB	0.6039	0.6840	0.648 1	0.5784	**0.8099**
	DT	0.6581	0.7552	0.8441	**0.8693**	0.8249
HCI	SVM	0.5323	0.5976	0.6771	**0.8700**	0.7631
	LSTM	0.7523	0.7124	**0.7726**	0.6950	0.6269
	GRU	0.7474	0.7193	**0.7493**	0.7109	0.7944
	NB	0.6378	**0.6648**	0.6064	0.5961	0.5923
	DT	0.9340	0.9332	**0.9481**	0.9436	**0.9481**
PS	SVM	0.5185	**0.5223**	0.5180	0.5180	**0.5228**
	LSTM	0.7277	**0.7777**	**0.7777**	**0.7777**	0.7759
	GRU	**0.8318**	0.8317	**0.8318**	0.8283	0.8283
	NB	**0.7516**	0.7155	0.6763	0.6679	0.6380
	DT	0.8097	0.8829	0.9161	**0.9604**	0.8821
WISDM	SVM	**0.8275**	0.8244	0.8191	0.811	0.8106
	LSTM	0.8333	0.8946	0.8900	0.9011	**0.9090**
	GRU	0.9365	0.953	**0.9562**	0.95214	0.9217
	NB	**0.6670**	0.6704	0.5283	0.2061	0.3059
	DT	**0.5984**	0.5428	0.5723	0.5130	0.5595
UCI	SVM	0.7374	0.7195	0.7623	0.6842	**0.7778**
	LSTM	0.9366	0.9158	0.8887	0.9210	**0.9490**
	GRU	**0.8114**	0.7194	0.5283	0.6935	0.6555

We select several different classification models to investigate the impact of time-based static window segmentation. The results of the time-based static segmentation technique for each *t* are shown in Table III.

As Table III demonstrates, on the SKODA dataset, DT and LSTM achieved the best F_1 values of 0.9657 and 0.9336, respectively, at *t*=10 s, while NB and SVM achieved the best F_1 values of 0.8292 and 0.9336, respectively, at *t*=5 s. The optimal window lengths chosen are different for the different methods. On the WISDM dataset, we found that NB and SVM achieved 0.7516 and 0.8275 F_1 values at *t*=1 s, while for DT and LSTM, the best results are achieved at *t*=5 and *t*=10 s. The longer the length of the window for the same dataset, the more information it contains, but it may fail to recognize the active transition points. Instead, the smaller the length of the window may capture the activity transition points but may misclassify them because the window does not contain enough key information.

From the above experimental results, we do not compare which method performs better at classification because we tested specific parameters on the five datasets. We investigate whether the length of the window affects the F_1 score of the method. We conclude that the optimal window length is different for different methods on the same dataset and the optimal window length chosen for the same method on different datasets also varies due to the variable duration of the activity on different datasets.
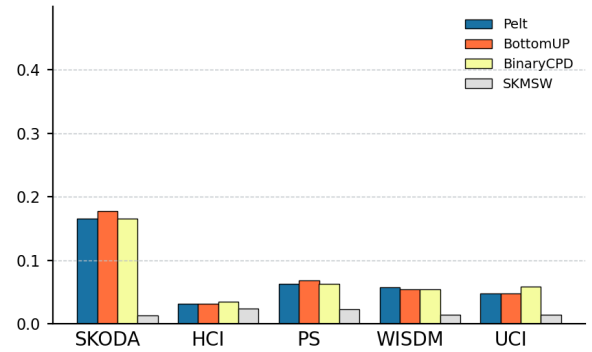

Fig. 5. NED performance on the five benchmarking datasets

D. Dynamic Segmentation

As shown in the above experiments based on static window segmentation, a suitable window length can improve the performance of classification, but in real life, choosing an optimal window length is difficult. Therefore, in this section, we use dynamic segmentation based on sensor data. We do not want to compare the segmentation performance with the following benchmark because it is slightly unfair. We attempt to investigate the relationship between segmentation accuracy and classification accuracy on the same dataset. The benchmark method uses dynamic segmentation followed by feature extraction. The feature extraction is fixed, and our method performs feature extraction followed by segmentation. The F_1 score of the segmentation methods is shown in Table IV.

Methods \ Datasets	SKODA	HCI	PS	WISDM	UCI
Dynp [23]	0.8858	0.8751	0.9663	0.8711	0.9352
BottomUP [53]	0.8661	0.8750	0.9536	0.8807	0.9353
BinaryCPD [54]	0.8826	0.8450	0.9601	0.8859	0.9151
MTHARS	**0.9648**	**0.9479**	**0.9733**	**0.9872**	**0.9632**

As shown in Table IV, the F_1 values of all the methods exceed 90% on both the PS and UCI datasets. However, the F_1 values of all the methods on the HCI dataset are lower than the accuracy of the remaining four datasets. Our proposed method is superior to the dynamic segmentation-based method, possibly because our method better identifies the starting and ending positions of the activity, which can improve the classification performance.

To verify our hypothesis, we investigated the relationship between the performance of the classification and the segmentation accuracy. The overall results of the segmentation performance are shown in Fig. 5. A smaller NED value means that the position of the segmented activity sequence is closer to the position of the real activity sequence. From Fig. 5, we can see that our method achieves the lowest NED values, and the classification performance is more accurate. on the HCI dataset, we find that the NED values of Dynp and BottomUP are similar, and their classification results are also close to each other. On the PS dataset, the NED values of Dynp and BinaryCPD are lower than those of the BottomUP method, and the F_1 score of their classifications is higher than that of the BottomUP classification. On the WISDM dataset, the BottomUP and BinaryCPD methods have higher classification results than Dynp, and their NED values are lower than those of the Dynp method.

From the above experimental results, it is indicated that precision in obtaining the start and end positions of the activities can improve the performance of the recognition activities. If data segmentation is considered as a preprocessing process, errors in data segmentation may be propagated to the later steps.

E. Activity Recognition

In this scenario, we investigate the classification performance of our method compared with SK [44]. For the baseline methods, we leverage the segmentation methods mentioned in their papers (sliding window methods are applied). The datasets were randomly divided into training and testing sets according to the experimental benchmark, where the training and testing sets in the PAMAP2 dataset were in a ratio of 80% and 20%, respectively, and the proportions of the training and testing sets in the remaining seven datasets were 70% and 30%, respectively. The missing values in the dataset were linearly interpolated or repeated from the previous values, and data preprocessing was performed by normalization.

Table V reports the experimental results of MTHARS and the baselines. To further evaluate the generality of our method, we ran the SK code using the same evaluation criteria (as shown in Table VI). The result shows that our proposed method outperforms the state-of-the-art performance.

1) Improvements on the SKODA dataset: Compared with SK [44], our method obtains a 0.22 % higher F_1 score. We also compare the MTHARS method with previously published results. To the best of our knowledge, the best result is [16], and the MTHARS method obtains a 0.52% higher F_1 score.

2) Improvements on the HCI dataset: The results show that our method outperforms SK [44] by obtaining a 1.47 % higher F_1 score.

3) Improvements on the PS dataset: When compared with SK [44], our method obtains a 1.47 % higher F_1 score.

4) Improvements on the WISDM dataset: Table V shows that the MTHARS outperforms the SK [44] method by a 1.52% higher F_1 score. Moreover, we can observe that the MTHARS attains a 1.57% higher F_1 score than the rest of the published results [43].

5) Boost on the UCI dataset: we compare the MTHARS with the SK [44] method on the test set. As shown in Table V, the MTHARS obtains a 1.65% improvement. We compare the MTHARS to the recently published results on the UCI dataset. According to our investigation, the best result thus far is 0.9660 [42], and the MTHARS obtains a 0.63% higher F_1 score.

6) Improvements on the OPPORTUNITY dataset: We still use the same method for comparison. In Table V, we show our experimental results that outperform the SK method with a 1.39% improvement on the test dataset. Then, we compare the results with the currently published studies as follows: [16], [56], [58], [60]. We can see from Table V that the MTHARS obtains 0.63%, 7.23%, 19.53% and 11.55% improvements compared to them, respectively. Compared to [40], the MTHARS results are closer to it.

7) Boost on the PAMAP2 dataset: According to Table V, the F_1 score of MTHARS surpasses that of SK on this dataset. Compared with the recently published results [58], [42], [60], the MTHARS obtains a 9.32%, 2.32% and 1.77% improvement. The confusion matrices have been computed in Fig.6 to visually show the performance improvements.

8) Boost on the UNIMIB SHAR dataset: We investigated the impact of our method on the experimental results. Table V shows that MTHARS receives a 1.08% boost compared to SK. We also compare MTHARS with other published research. From our investigation, the best value on the UNIMIB SHAR dataset is [42], with which the MTHARS obtains a 0.33% improvement.

From the above results, we concluded that the MTHARS method, performing activity segmentation and recognition simultaneously, is able to improve the accuracy of activity classification. Segmentation of the activity by employing multiscale windows can provide an accurate boundary for recognizing the activity. Moreover, the two tasks can mutually facilitate each other.

TABLE V
F_1 PERFORMANCE ON EIGHT DATA SETS.

Methods \ Dataset	SKODA	HCI	PS	WISDM	UCI	OPPORTUNITY	PAMAP2	UNIMIB SHAR
SK [44]	0.9510	0.9377	0.9574	0.9725	0.9558	0.9074	0.9338	0.7463
MTHARS	**0.9632**	**0.9524**	**0.9721**	**0.9877**	**0.9723**	**0.9213**	**0.9480**	**0.7571**
Other Reachers	0.958* [16]			0.9263 [40]	0.9302 [37]	0.915 [16]	0.9248 [42]	0.7538 [42]
	0.928 [55]			0.949 [56]	0.9585 [40]	0.9263 [40]	0.9116 [57]	
	0.924 [58]			0.9720 [43]	0.9545 [41]	0.849 [56]	0.908 [55]	
	0.916 [59]				0.9660 [42]	0.746 [55]	0.854 [58]	
					0.9537 [43]	0.726 [58]	0.9303 [60]	
					0.9293 [57]	0.8058 [60]		

TABLE VI
ACCURACY PERFORMANCE ON EIGHT DATASETS.

Methods \ Dataset	SKODA	HCI	PS	WISDM	UCI	OPPORTUNITY	PAMAP2	UNIMIB SHAR
SK [44]	0.9586	0.9341	0.9649	0.9751	0.9406	0.9014	0.9380	0.7589
MTHARS	**0.9648**	**0.9479**	**0.9733**	**0.9872**	**0.9632**	**0.9153**	**0.9450**	**0.7648**

F. Ablation experiments

In this subsection, we conduct ablation experiments on the benchmarking datasets to investigate the effectiveness of the approach. During our experiments, we found that the class loss and offset loss weights and the scale s of the window are two essential settings.

First, the weights α and β represent the different proportions of class loss and offset loss in the loss calculation. For simplicity, we first set the scale s of the window to 2 and 3. To investigate how they affect the experimental classification results, we considered different values of the weights α and β on the OPPORTUNITY and WISDM datasets. We considered that when $\alpha=1$ $\beta=1$, $\alpha=1$ $\beta=2$, $\alpha=1$ $\beta=3$, $\alpha=2$ $\beta=1$. The detailed results of the experiment are shown in Table VII. From the table, we can see that the best result on the WISDM dataset is the combination of $\alpha=2$ $\beta=3$. In addition, when $\alpha=2$, $\beta=3$ is very similar to the result when $\alpha=1$ $\beta=1$. The value of 0.9796 when $\alpha=1$ $\beta=2$ is very close to the result of 0.9783 when $\alpha=2$ $\beta=1$. On the OPPORTUNITY dataset, we can see from the table that $\alpha=1$ $\beta=3$ is close to the results for two different combinations of $\alpha=2$ $\beta=3$, $\alpha=1$ $\beta=1$.
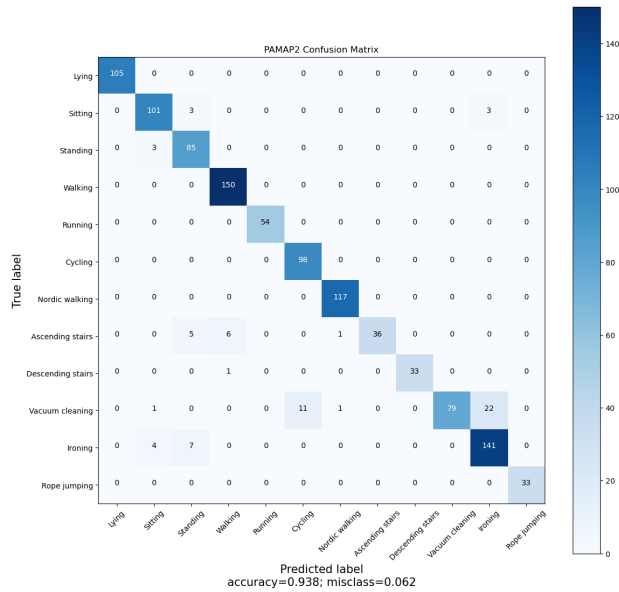
TABLE VII
ACTIVITY CLASSIFICATION F_1 VALUE WITH DIFFERENT WEIGHT
SETTINGS ON DIFFERENT DATA SETS

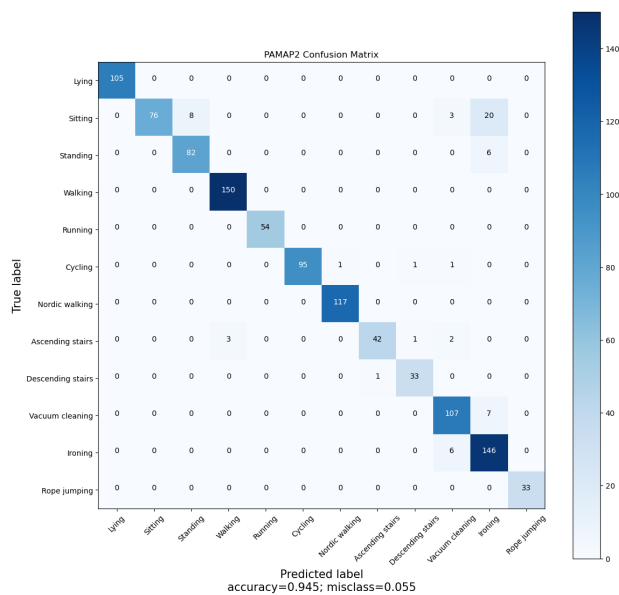| Model	OPPORTUNITY	WISDM
SK [44]	0.9074	0.9725
$\alpha=1,\beta=1$	**0.9213**	0.9877
$\alpha=1,\beta=2$	0.9060	0.9796
$\alpha=1,\beta=3$	0.9174	0.9874
$\alpha=2,\beta=1$	0.9075	0.9783
$\alpha=2,\beta=3$	0.9154	**0.9881**

Next, we seek to better understand the effect of different sizes and numbers of scale s on the experimental classification results. Therefore, we set various numbers and scales s on the OPPORTUNITY and UCI datasets. We believe that different sizes and numbers of scale s generating the number and length of windows are different. Different numbers and lengths of windows produce different offset values from the true activity boundary, which will have an impact on the experimental results. Due to the dataset length limitation, we only set it when there is only one $s=2$, $s=2$, 3, $s=0.5$, 0.3 and $s=2$, 3, 4, respectively. Specifically, the weights α and β are set to 1. The detailed results of the experimental classification are shown in Table VIII. We found that when only one s is set, the effect is not as good as the classification effect when several different s are set. On the OPPORTUNITY dataset, setting the scale too small, such as $s = 0.5$ and 0.3, is close to the classification result of $s=2$. Setting the scale too large, such as $s=4$, is close to the experimental classification result of $s=0.5$, 0.3. The best classification effect is to set the scale to $s=2$, 3. On the UCI dataset, the best result is 0.9723 when $s=2$, 3, 4. The second result is 0.9615 with $s=2$, 3. The results show that combining classification and segmentation using multiple windows of different scales results in better recognition of activities of different lengths.

V. CONCLUSION AND FUTURE WORK

Accurate segmentation of activities, as well as recognition of activities, is a challenging task. In this paper, we propose a method called MTHARS, which generates multiscale windows to segment activities of different lengths. MTHARS combines activity segmentation and recognition, which not only improves the activity segmentation performance but also im-

proves the accuracy of classification. We evaluated the method on eight benchmark datasets and our method outperformed the state-of-the-art methods. To verify the effectiveness of the method, we conducted several ablation experiments on the benchmark dataset. Future research could be conducted to improve the model's performance on activity boundaries with very short durations.

References

[1] L. Chen, J. Hoey, C. D. Nugent, D. J. Cook, and Z. Yu, "Sensor-based activity recognition," *IEEE Transactions on Systems, Man, and Cybernetics, Part C (Applications and Reviews)*, vol. 42, no. 6, pp. 790–808, 2012.

[2] L. Chen, C. D. Nugent, and H. Wang, "A knowledge-driven approach to activity recognition in smart homes," *IEEE Transactions on Knowledge and Data Engineering*, vol. 24, no. 6, pp. 961–974, 2011.

[3] D. J. Cook, J. C. Augusto, and V. R. Jakkula, "Ambient intelligence: Technologies, applications, and opportunities," *Pervasive and Mobile Computing*, vol. 5, no. 4, pp. 277–298, 2009.

[4] O. D. Lara and M. A. Labrador, "A survey on human activity recognition using wearable sensors," *IEEE communications surveys & tutorials*, vol. 15, no. 3, pp. 1192–1209, 2012.

[5] N. C. Krishnan and D. J. Cook, "Activity recognition on streaming sensor data," *Pervasive and mobile computing*, vol. 10, pp. 138–154, 2014.

[6] Z. Wang, N. Yang, M. Guo, and H. Zhao, "Human-human interactional synchrony analysis based on body sensor networks," *IEEE Transactions on Affective Computing*, vol. 10, no. 3, pp. 407–416, 2017.

[7] E. Kim, S. Helal, and D. Cook, "Human activity recognition and pattern discovery," *IEEE pervasive computing*, vol. 9, no. 1, pp. 48–53, 2009.

[8] P. Rashidi, D. J. Cook, L. B. Holder, and M. Schmitter-Edgecombe, "Discovering activities to recognize and track in a smart environment," *IEEE transactions on knowledge and data engineering*, vol. 23, no. 4, pp. 527–539, 2010.

[9] G. Acampora, D. J. Cook, P. Rashidi, and A. V. Vasilakos, "A survey on ambient intelligence in healthcare," *Proceedings of the IEEE*, vol. 101, no. 12, pp. 2470–2494, 2013.

[10] M. H. M. Noor, Z. Salcic, I. Kevin, and K. Wang, "Adaptive sliding window segmentation for physical activity recognition using a single tri-axial accelerometer," *Pervasive and Mobile Computing*, vol. 38, pp. 41–59, 2017.

[11] G. Okeyo, L. Chen, H. Wang, and R. Sterritt, "Dynamic sensor data segmentation for real-time knowledge-driven activity recognition," *Pervasive and Mobile Computing*, vol. 10, pp. 155–172, 2014.

[12] J. Wang, T. Zhu, J. Gan, H. Ning, and Y. Wan, "Sensor data augmentation with resampling for contrastive learning in human activity recognition," *arXiv preprint arXiv:2109.02054*, 2021.

[13] J. Wang, T. Zhu, L. Chen, H. Ning, and Y. Wan, "Negative selection by clustering for contrastive learning in human activity recognition," *arXiv preprint arXiv:2203.12230*, 2022.

[14] C. A. Ronao and S.-B. Cho, "Human activity recognition with smartphone sensors using deep learning neural networks," *Expert systems with applications*, vol. 59, pp. 235–244, 2016.

[15] S. Hochreiter and J. Schmidhuber, "Long short-term memory," *Neural computation*, vol. 9, no. 8, pp. 1735–1780, 1997.

[16] F. J. Ordóñez and D. Roggen, "Deep convolutional and lstm recurrent neural networks for multimodal wearable activity recognition," *Sensors*, vol. 16, no. 1, p. 115, 2016.

[17] W. Zhang, T. Zhu, C. Yang, J. Xiao, and H. Ning, "Sensors-based human activity recognition with convolutional neural network and attention mechanism," in *2020 IEEE 11th International Conference on Software Engineering and Service Science (ICSESS)*. IEEE, 2020, pp. 158–162.

[18] H. Qian, S. J. Pan, and C. Miao, "Weakly-supervised sensor-based activity segmentation and recognition via learning from distributions," *Artificial Intelligence*, vol. 292, p. 103429, 2021.

[19] W. Liu, D. Anguelov, D. Erhan, C. Szegedy, S. Reed, C.-Y. Fu, and A. C. Berg, "Ssd: Single shot multibox detector," in *European conference on computer vision*. Springer, 2016, pp. 21–37.

[20] R. Girshick, J. Donahue, T. Darrell, and J. Malik, "Rich feature hierarchies for accurate object detection and semantic segmentation," in *Proceedings of the IEEE conference on computer vision and pattern recognition*, 2014, pp. 580–587.

Fig. 6. The confusion matrices on the PAMAP2 dataset between SK [44] and MTHARS. (a) SK, (b) MTHARS

TABLE VIII
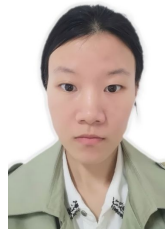ACTIVITY CLASSIFICATION F_1 VALUE FOR DIFFERENT s ON DIFFERENT DATASET

Model	OPPORTUNITY	UCI
SK [44]	0.9074	0.9558
s=2	0.9138	0.9505
s=0.5,0.3	0.9160	0.8928
s=2,3	**0.9213**	0.9615
s=2,3,4	0.9167	**0.9723**

[21] S. Aminikhanghahi, T. Wang, and D. J. Cook, "Real-time change point detection with application to smart home time series data," *IEEE Transactions on Knowledge and Data Engineering*, vol. 31, no. 5, pp. 1010–1023, 2018.

[22] S. Aminikhanghahi and D. J. Cook, "A survey of methods for time series change point detection," *Knowledge and information systems*, vol. 51, no. 2, pp. 339–367, 2017.

[23] Y. Guédon, "Exploring the latent segmentation space for the assessment of multiple change-point models," *Computational Statistics*, vol. 28, no. 6, pp. 2641–2678, 2013.

[24] K. Chen, D. Zhang, L. Yao, B. Guo, Z. Yu, and Y. Liu, "Deep learning for sensor-based human activity recognition: Overview, challenges, and opportunities," *ACM Computing Surveys (CSUR)*, vol. 54, no. 4, pp. 1–40, 2021.

[25] L. Wang, T. Gu, X. Tao, and J. Lu, "A hierarchical approach to real-time activity recognition in body sensor networks," *Pervasive and Mobile Computing*, vol. 8, no. 1, pp. 115–130, 2012.

[26] O. Banos, J.-M. Galvez, M. Damas, H. Pomares, and I. Rojas, "Window size impact in human activity recognition," *Sensors*, vol. 14, no. 4, pp. 6474–6499, 2014.

[27] J. Wan, M. J. OâĂŹgrady, and G. M. OâĂŹHare, "Dynamic sensor event segmentation for real-time activity recognition in a smart home context," *Personal and Ubiquitous Computing*, vol. 19, no. 2, pp. 287–301, 2015.

[28] H. Li, G. D. Abowd, and T. Plötz, "On specialized window lengths and detector based human activity recognition," in *Proceedings of the 2018 ACM international symposium on wearable computers*, 2018, pp. 68–71.

[29] L. Santos, K. Khoshhal, and J. Dias, "Trajectory-based human action segmentation," *Pattern Recognition*, vol. 48, no. 2, pp. 568–579, 2015.

[30] C. Ma, W. Li, J. Cao, J. Du, Q. Li, and R. Gravina, "Adaptive sliding window based activity recognition for assisted livings," *Information Fusion*, vol. 53, pp. 55–65, 2020.

[31] J. Ye, G. Stevenson, and S. Dobson, "Kcar: A knowledge-driven approach for concurrent activity recognition," *Pervasive and Mobile Computing*, vol. 19, pp. 47–70, 2015.

[32] D. Triboan, L. Chen, F. Chen, and Z. Wang, "Semantic segmentation of real-time sensor data stream for complex activity recognition," *Personal and Ubiquitous Computing*, vol. 21, no. 3, pp. 411–425, 2017.

[33] ——, "A semantics-based approach to sensor data segmentation in real-time activity recognition," *Future Generation Computer Systems*, vol. 93, pp. 224–236, 2019.

[34] V. Bianchi, M. Bassoli, G. Lombardo, P. Fornacciari, M. Mordonini, and I. De Munari, "Iot wearable sensor and deep learning: An integrated approach for personalized human activity recognition in a smart home environment," *IEEE Internet of Things Journal*, vol. 6, no. 5, pp. 8553–8562, 2019.

[35] M. Gil-Martín, R. San-Segundo, F. Fernandez-Martinez, and J. Ferreiros-López, "Improving physical activity recognition using a new deep learning architecture and post-processing techniques," *Engineering Applications of Artificial Intelligence*, vol. 92, p. 103679, 2020.

[36] C. Pham, S. Nguyen-Thai, H. Tran-Quang, S. Tran, H. Vu, T.-H. Tran, and T.-L. Le, "Senscapsnet: deep neural network for non-obtrusive sensing based human activity recognition," *IEEE Access*, vol. 8, pp. 86 934–86 946, 2020.

[37] F. Cruciani, A. Vafeiadis, C. Nugent, I. Cleland, P. McCullagh, K. Votis, D. Giakoumis, D. Tzovaras, L. Chen, and R. Hamzaoui, "Feature learning for human activity recognition using convolutional neural networks," *CCF Transactions on Pervasive Computing and Interaction*, vol. 2, no. 1, pp. 18–32, 2020.

[38] W. Huang, L. Zhang, W. Gao, F. Min, and J. He, "Shallow convolutional neural networks for human activity recognition using wearable sensors," *IEEE Transactions on Instrumentation and Measurement*, vol. 70, pp. 1–11, 2021.

[39] C. Xu, D. Chai, J. He, X. Zhang, and S. Duan, "Innohar: A deep neural network for complex human activity recognition," *Ieee Access*, vol. 7, pp. 9893–9902, 2019.

[40] K. Xia, J. Huang, and H. Wang, "Lstm-cnn architecture for human activity recognition," *IEEE Access*, vol. 8, pp. 56 855–56 866, 2020.

[41] L. Tong, H. Ma, Q. Lin, J. He, and L. Peng, "A novel deep learning bi-gru-i model for real-time human activity recognition using inertial sensors," *IEEE Sensors Journal*, 2022.

[42] Y. Tang, L. Zhang, Q. Teng, F. Min, and A. Song, "Triple cross-domain attention on human activity recognition using wearable sensors," *IEEE Transactions on Emerging Topics in Computational Intelligence*, 2022.

[43] Z. N. Khan and J. Ahmad, "Attention induced multi-head convolutional neural network for human activity recognition," *Applied Soft Computing*, vol. 110, 10 2021.

[44] W. Gao, L. Zhang, W. Huang, F. Min, J. He, and A. Song, "Deep neural networks for sensor-based human activity recognition using selective kernel convolution," *IEEE Transactions on Instrumentation and Measurement*, vol. 70, pp. 1–13, 2021.

[45] T. Stiefmeier, D. Roggen, and G. Troster, "Fusion of string-matched templates for continuous activity recognition," in *2007 11th IEEE International Symposium on Wearable Computers*. IEEE, 2007, pp. 41–44.

[46] K. Forster, D. Roggen, and G. Troster, "Unsupervised classifier self-calibration through repeated context occurences: Is there robustness against sensor displacement to gain?" in *2009 international symposium on wearable computers*. IEEE, 2009, pp. 77–84.

[47] M. Shoaib, S. Bosch, O. D. Incel, H. Scholten, and P. J. Havinga, "Fusion of smartphone motion sensors for physical activity recognition," *Sensors*, vol. 14, no. 6, pp. 10 146–10 176, 2014.

[48] J. R. Kwapisz, G. M. Weiss, and S. A. Moore, "Activity recognition using cell phone accelerometers," *ACM SigKDD Explorations Newsletter*, vol. 12, no. 2, pp. 74–82, 2011.

[49] D. Anguita, A. Ghio, L. Oneto, X. Parra Perez, and J. L. Reyes Ortiz, "A public domain dataset for human activity recognition using smartphones," in *Proceedings of the 21th international European symposium on artificial neural networks, computational intelligence and machine learning*, 2013, pp. 437–442.

[50] A. Reiss and D. Stricker, "Introducing a new benchmarked dataset for activity monitoring," in *2012 16th international symposium on wearable computers*. IEEE, 2012, pp. 108–109.

[51] D. Micucci, M. Mobilio, and P. Napoletano, "Unimib shar: A dataset for human activity recognition using acceleration data from smartphones," *Applied Sciences*, vol. 7, no. 10, p. 1101, 2017.

[52] S. Aminikhanghahi and D. J. Cook, "Enhancing activity recognition using cpd-based activity segmentation," *Pervasive and Mobile Computing*, vol. 53, pp. 75–89, 2019.

[53] E. Keogh, S. Chu, D. Hart, and M. Pazzani, "An online algorithm for segmenting time series," in *Proceedings 2001 IEEE international conference on data mining*. IEEE, 2001, pp. 289–296.

[54] P. Fryzlewicz, "Wild binary segmentation for multiple change-point detection," *The Annals of Statistics*, vol. 42, no. 6, pp. 2243–2281, 2014.

[55] A. Abedin, M. Ehsanpour, Q. Shi, H. Rezatofighi, and D. C. Ranasinghe, "Attend and discriminate: Beyond the state-of-the-art for human activity recognition using wearable sensors," *Proceedings of the ACM on Interactive, Mobile, Wearable and Ubiquitous Technologies*, vol. 5, no. 1, pp. 1–22, 2021.

[56] A. A. Varamin, E. Abbasnejad, Q. Shi, D. C. Ranasinghe, and H. Rezatofighi, "Deep auto-set: A deep auto-encoder-set network for activity recognition using wearables," in *Proceedings of the 15th EAI International Conference on Mobile and Ubiquitous Systems: Computing, Networking and Services*, 2018, pp. 246–253.

[57] S. Wan, L. Qi, X. Xu, C. Tong, and Z. Gu, "Deep learning models for real-time human activity recognition with smartphones," *Mobile Networks and Applications*, vol. 25, no. 2, pp. 743–755, 2020.

[58] Y. Guan and T. Plötz, "Ensembles of deep lstm learners for activity recognition using wearables," *Proceedings of the ACM on Interactive, Mobile, Wearable and Ubiquitous Technologies*, vol. 1, no. 2, pp. 1–28, 2017.

[59] R. Yao, G. Lin, Q. Shi, and D. C. Ranasinghe, "Efficient dense labelling of human activity sequences from wearables using fully convolutional networks," *Pattern Recognition*, vol. 78, pp. 252–266, 2018.

[60] Q. Teng, K. Wang, L. Zhang, and J. He, "The layer-wise training convolutional neural networks using local loss for sensor-based human activity recognition," *IEEE Sensors Journal*, vol. 20, no. 13, pp. 7265–7274, 2020.

Furong Duan received his B.E. degree from Hengyang Normal University in 2019. Her is currently a M.S. student in the School of Computer Science, University of South China. His research interests include intelligent perception and pattern recognition.

Tao Zhu received his B.E. degree from Central South University, Changsha, China, and Ph.D. from University of Science and Technology of China, Hefei, China, in 2009 and 2015 respectively. He is currently an associate professor at University of South China, Hengyang, China. He is the principal investigator of several projects funded by the National Natural Science Foundation of China and Science Foundation of Hunan Province etc. He is now the Chair of IEEE CIS Smart World Technical Committee Task Force on "User-Centred Smart Systems".His research interests include IoT, pervasive computing, assisted living and evolutionary computation.

Jinqiang Wang received his B.E. degree from Henan Normal University in 2020. He is currently a M.S. student in the School of Computer Science, University of South China. His research interests include intelligent perception and pattern recognition.